ACS APPLIED ENERGY MATERIALS

www.acsaem.org

Article

Can 2D Carbon Allotropes Be Used as Photovoltaic Absorbers in Solar Harvesting Devices?

Alexandre Cavalheiro Dias,* Carlos Derli Almeida Cornélio, Maurício Jeomar Piotrowski, Luiz Antônio Ribeiro Júnior, Carlos Maciel de Oliveira Bastos, Celso Ricardo Caldeira Rêgo, and Diego Guedes-Sobrinho*

Cite This: https://doi.org/10.1021/acsaem.4c01544

Read Online

ACCESS | Metrics & More | Article Recommendations | Supporting Information

ABSTRACT: Sustainable energy solutions have led to extensive research into materials for the conversion of solar energy. Two-dimensional carbon allotropes have garnered significant attention due to their unique structural and electronic properties, which can enhance the efficiency and sustainability of solar panels. This study used several computational methods, including density functional theory, density functional tight binding, and molecular dynamics simulations, to explore the solar energy conversion capabilities of 30 different 2D carbon-based allotropes. After a thorough analysis, we found that these materials exhibited a wide range of power conversion efficiency values, from 7% to 30%, assuming complete absorption of incident light. Our research provides valuable insights into the structural and electronic properties that impact the performance of these materials in solar cell applications.

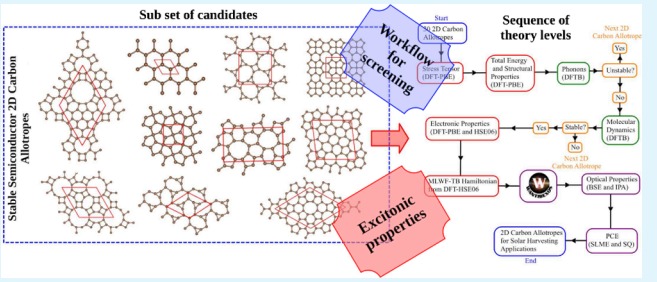

KEYWORDS: *Density functional theory, Tight-binding, Wannier functions, Excitons, Electronic and optical properties, 2D materials, Carbon allotropes*

1. INTRODUCTION

The rapid advancement of nanoscience has revolutionized material design for various energy storage and conversion applications.[1−3] The groundbreaking synthesis of graphene marked a pivotal moment, igniting a wave of exploration within nanoelectronics.[4] Graphene's exceptional traits, including its lightweight composition, formidable mechanical resilience, optical transparency, and unparalleled electrical and thermal conductivity, have captivated researchers' attention.[5,6] This milestone has spurred extensive experimental[7,8] and theoretical[9,10] inquiries into novel 2D carbon allotropes. The primary objective is to engineer all-carbon 2D materials replicating graphene's remarkable properties while overcoming its limitations, particularly the absence of an electronic band gap.[11] This pursuit has culminated in a multifaceted approach, blending computational screening with experimental endeavors to unveil alternatives poised to redefine flat electronics.

The physicochemical properties of all-carbon 2D materials are intricately tied to the synthesis process, offering a realm of controllability.[12,13] Based on this, numerous candidates have emerged, each presenting a unique suite of characteristics.[14−16] Among these materials, several have transcended theoretical speculation to become experimental realities.[17,18] Noteworthy examples include monolayer amorphous carbon (MAC),[17] the 2D biphenylene network (BPN),[19] the monolayer fullerene network ($2DC_{60}$),[18] and multilayer γ-graphyne.[20]

MAC and BPN exhibit similarities with graphene, revealing a zero semimetal band gap and Dirac cones indicative of linear dispersion.[17,18,21−23] However, they differ significantly in their structural compositions.[24,25] MAC is characterized by randomly distributed defects with carbon rings of varying sizes (five, six, seven, and eight atoms), which present a lattice distinct from that of disordered graphene. In contrast, BPN features a periodic arrangement of four-, six-, and eight-carbon rings. On another front, γ-Graphyne and $2DC_{60}$ address the zero band gap limitation common in other 2D carbon materials, making them suitable for digital electronics applications. γ-Graphyne has a small direct bandgap of 0.48 eV,[20] while $2DC_{60}$ demonstrates a direct semiconducting band gap of 1.6 eV.[26] The crystalline structure of $2DC_{60}$ arises from covalently bonded C_{60} polymers arranged in a planar configuration, yielding stable crystals with quasi-hexagonal and quasi-tetragonal phases.[27] This innovative clustering

Received: June 16, 2024
Revised: August 21, 2024
Accepted: August 29, 2024

mechanism opens new avenues for tailoring the electronic properties of 2D carbon-based materials.

Integrating computational approaches into material design has become indispensable in contemporary research, driven by several compelling factors.[28] Often, theoretical predictions of novel nanostructured materials precede their experimental realization by years or even decades. For example, BPN and the 2D monolayer of C_{60} were first theoretically explored by Mortazavi in 2017[22] and Tomanek in 1990,[29] respectively. Computational models facilitate the simulation and prediction of material properties, enabling virtual experiments that accelerate the discovery and development of new materials. Researchers gain unprecedented access to materials' underlying physics and chemistry through computational simulation protocols, unveiling insights into their atomic-scale structures, electronic properties, and intermolecular interactions. This profound understanding not only elucidates the fundamental mechanisms governing material behavior but also informs the strategic design of materials tailored to specific applications.

Using 2D carbon allotropes as photo absorbers in solar harvesting devices represents a frontier in green energy solutions. Despite the growing interest in 2D materials for various applications, their potential in photovoltaics still needs to be explored. Our study aims to investigate the intricate interplay between 2D carbon allotropes and solar energy conversion. By elucidating the photoabsorption properties of these materials and their efficiency in converting sunlight into usable electrical energy, our research seeks to unlock new avenues for enhancing the efficiency and sustainability of solar harvesting technologies.

In this study, we employed a comprehensive computational approach to explore the potential of 2D carbon allotropes as pivotal elements in the advancement of next-generation solar cells. Using a suite of methodologies, including density functional theory (DFT), density functional tight binding (DFTB), and molecular dynamics (MD) simulations, we devised a screening procedure to assess the solar harvesting efficiency of 30 distinct 2D carbon-based allotropes. Our analyses focused on calculating their power conversion efficiency (PCE), providing insight into their viability for solar energy conversion. The results reveal a spectrum of PCE values ranging from 7% to 30% when the maximum absorbance is considered, highlighting the diverse potential of these materials. Through these computational findings, our study aims to illuminate the performance landscape of 2D carbon allotropes and inspire further exploration and innovation in renewable energy technologies.

2. COMPUTATIONAL EXPERIMENTS

2.1. Computational Details. Our computational simulations for structural and total energy optimization were performed using DFT,[30,31] implemented in the Vienna *Ab Initio* Simulation Package (VASP).[32] For the description of electronic and structural properties, we utilized the semilocal exchange-correlation functional via the generalized gradient approximation (GGA)[33] as proposed by Perdew–Burke–Ernzerhof (PBE).[34] However, it is known that PBE underestimates the electronic band gap,[35,36] owing to self-interaction problems and a poor description of weak interactions.[37] To obtain a more realistic description of the electronic band gap, we adopted the screened Coulomb hybrid exchange-correlation functional proposed by Heyd–Scuseria–Ernzerhof (HSE06).[38]

The Kohn–Sham (KS) equations were solved using the projector augmented wave (PAW) method,[39] where the KS states were expanded in plane waves. The equilibrium structure was obtained through stress tensor optimization and atomic force minimization, employing a cutoff energy of 827.984 eV. Atomic forces were kept below 0.01 eVÅ^{-1}, and a total energy criterion of 10^{-6} eV was enforced in the KS self-consistent cycle. We employed a cutoff energy of 465.741 eV with the same simulation parameters for the rest of the electronic properties. Brillouin Zone integration was performed using a **k**-points density of 40 Å^{-1} in each reciprocal lattice vector direction in the *xy* plane. To prevent unwanted interactions between the 2D carbon allotrope and its periodic images in the $\hat{Z}$ direction, we employed a vacuum thickness of 20 Å, as these 2D carbon allotropes were constructed with *xy* periodicity.

The phonon dispersion was obtained using DFTB with self-consistent charge (SCC),[40] combining the DFTB+ code[41] and the Phonopy package.[42] We used the finite displacement method with a 4 × 4 × 1 supercell and a 4 × 4 × 1 **k**-mesh. The 2D carbon allotropes were described within the DFTB framework using the Slater–Koster (SK) parametrization proposed by Gaus and co-workers.[43]

The MD simulations were performed using the SCC-DFTB method,[40] with the same SK parameters as before. We employed the Berendsen thermostat[44] for approximately 22 ps, with a time step of 1 fs. The temperature profile used for our MD simulations was as follows: (i) 1 ps from 0 to 400 K, (ii) 10 ps at 400 K, (iii) 1 ps from 400 to 300 K, and (iv) 10 ps at 300 K. We chose temperature profiles of 300 and 400 K, which are reasonable temperatures for solar cell operation. These simulations used supercells with approximately 300 atoms each and a 3 × 3 × 1 **k**-mesh.

To investigate the optical, excitonic, and solar harvesting properties of these systems, we utilized the WanTiBEXOS package developed in our group,[45] which enables the solution of the Bethe–Salpeter equation (BSE).[46] We employed a maximally localized Wannier function tight-binding (MLWF-TB) Hamiltonian, obtained from DFT HSE06 simulations using the Wannier90 package,[47] with *s* and *p* projections for carbon atoms. The BSE was solved using a 2D truncated Coulomb potential (V2DT),[48] with a **k**-points density of 120 Å^{-1} in each reciprocal lattice vector direction in the *xy* plane. Sufficient numbers of conduction and valence bands were considered to describe the absorption spectrum at both BSE and independent particle approximation (IPA) levels within the solar emission spectrum range (0.5 to 4.0 eV).[49] Further details regarding the employed parameters are provided in Supporting Information, Table S4.

The solar harvesting efficiency of these systems is estimated using the PCE, which considers the AM1.5G model for the solar emission spectrum,[49] employing both the Shockley–Queisser (SQ) limit[50] and the spectroscopy limited maximum efficiency (SLME) method.[51] These calculations were conducted based on the absorption spectrum obtained from both BSE and independent particle approximation (IPA) levels, with the solar cell operating at 298.15 K. The absorbance of these 2D carbon allotropes was evaluated by considering the total absorption coefficient spectrum obtained through the summation of dielectric function diagonal components. In our simulations, we assumed a monolayer thickness equal to the materials' thickness plus the van der Waals (vdW) length (i.e., 3.21 Å), as detailed in Supporting Information, Tables S6 and S7, consistent with prior

https://doi.org/10.1021/acsaem.4c01544
ACS Appl. Energy Mater. XXXX, XXX, XXX–XXX

studies.[52−54] The addition of vdW length to monolayer thickness is justified in the work of Bernardi et al.,[55] where this procedure is necessary to estimate graphene's absorbance due their atomic layer thickness, in order to reach results closer to experimental measures. Further, theoretical formalism's for SLME and the SQ limit can be found in previous works.[45,54]

2.2. Screening Procedure. The simulation protocol of the screening procedure used in this study is illustrated in Figure 1.

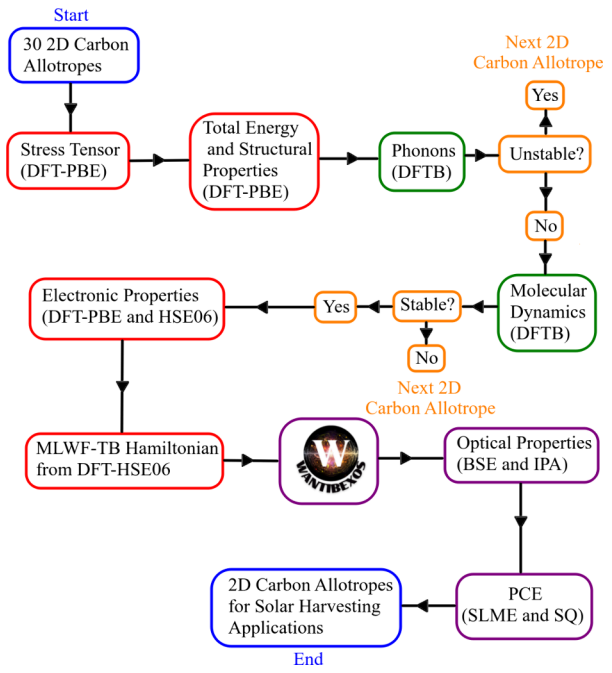

Figure 1. Workflow shows the screening procedure.

Initially, we selected 30 2D carbon allotropes (Figure 2), comprising 27 from a 2D carbon allotropes database,[56] and the remaining three from literature sources: Hexatetra-Carbon (HT-GRA),[57] Me graphene (Me-GRA),[58] and Pentagraphene (Penta-GRA).[59] Selection criteria included: (i) designation as a semiconductor with a band gap exceeding 0.5 eV and (ii) unit cell containing equal to or fewer than 40 atoms. Table S2, in Supporting Information, provides a correspondence between the 2D carbon allotrope names from the database[56] and the names adopted in this work, along with justifications for each adopted name. We conducted structural optimization with the set of 30 2D allotropes depicted in Figure 2. We analyzed their energetic and structural properties using DFT, specifically within the PBE exchange-correlation functional framework implemented in the VASP.

To assess these systems' structural and thermodynamic stability, we initially conducted phonon dispersion calculations using the DFTB approach, utilizing the DFTB+ code in conjunction with the Phonopy package. Based on the phonon results, we classified these systems as stable (ST), semistable (SS), or unstable (UN), following the criteria proposed by Inui et al.,[60] where stable systems exhibit no imaginary frequencies (represented as negative values in the phonon dispersion), or if present, such negative values around the Γ point are less than 1% of the highest frequency. Semistable systems possess small imaginary frequencies, primarily near the Γ point, which is lower than 10% of the highest frequency, and their vibrational modes are primarily acoustic. We also classify as semistable any systems meeting the characteristics above but also exhibiting imaginary frequencies in other **k**-points, with values lower than 1% of the highest frequency. Any systems failing to meet these criteria are considered unstable. Furthermore, we conducted MD simulations within the DFTB approach (MD-DFTB)[40] using the DFTB+ code, explicitly focusing on the ST and SS systems to investigate their dynamic stability under finite-temperature conditions.

From the thermodynamically stable systems confirmed by phonon and MD simulations, we computed their electronic properties, including the band gap and band structure, using the PBE and HSE06 functionals. For the HSE06 band structure, we utilized maximally localized Wannier functions (MLWF) obtained through the Wannier90 code, which yields a TB Hamiltonian. This TB Hamiltonian was then employed to investigate these systems' optical and excitonic properties using the WanTiBEXOS code. We identified semiconducting behavior among the stable allotropes based on the electronic properties, focusing solely on this subset to further investigate their excitonic and optical properties. Finally, we estimated the PCE of this subset using the SQ-limit and SLME approximations, aiming to identify suitable candidates for solar-harvesting applications.

3. RESULTS AND DISCUSSION

3.1. Structural Stability. All investigated 2D semiconductor carbon allotropes are depicted by their unit cells (red lines) in Figure 2. Complementary information about their structural characteristics, based on effective coordination number (ECN) and average weighted bond length (d_{av}),[61] was determined. For methodological details, refer to the Supporting Information. Among the configurations, HT-GRA, Penta-GRA, and Me-GRA are the only quasi-2D configurations. These allotropes exhibit an ECN > 3.00 and are impacted by the presence of atoms out of the plane, influencing them with C-sp^3 characteristics. In contrast, all the other configurations are formed by a single layer of atoms, allotropically coordinated, and present an ECN of 2.73−2.94, primarily based on C-sp^2.

The isomers are sequentially depicted from the least stable to the most stable. For instance, HT-GRA, with the highest relative energy of E_{rel} = 1.02 eV concerning OPH-GRA (0.00 eV), establishes the upper limit for all isomers within this range. Based solely on the E_{rel} values, allotropes could be classified into degeneracy groups for systems where E_{rel} < 0.03 eV. These groupings are as follows: (i) ΔE_{rel} = 0.01 eV for ORL3 concerning Liskene, also observed for TL-GRA, HPS, and HPS'-GRA isomers; (ii) ST-GRA has a ΔE_{rel} = 0.02 eV higher than SLO-GRA, and the same is observed for HP-GRA concerning SOI-GRA, as well as for OPI-GRA, ORL2, and Me-GRA; (iii) ScH-, ORL0, and OCD-GRA have an energy difference of ΔE_{rel} = 0.02 eV; (iv) ΔE_{rel} = 0.03 eV for ROPS, ORL1, HPS-GRA, and OI-GRA. The other allotropes not mentioned, exceeding a ΔE_{rel} = 0.03 eV, are more energetically separated, such as Liskene-D, K-GRA, PENTA-GRA, ORL4, OF-GRA, PHI-GRA, DPH-GRA, and OPH-GRA. However, while these groupings suggest some degeneracy among the isomers, this approach does not provide intrinsic thermodynamic stability for each isomer.

The thermodynamic stability of the carbon allotropes was assessed through a phonon dispersion analysis. Negative frequencies, indicating imaginary crystal vibrational modes, led to the classification of structures as SS or UN, as elaborated in Section 2.2. Conversely, structures with no negative

https://doi.org/10.1021/acsaem.4c01544
ACS Appl. Energy Mater. XXXX, XXX, XXX−XXX

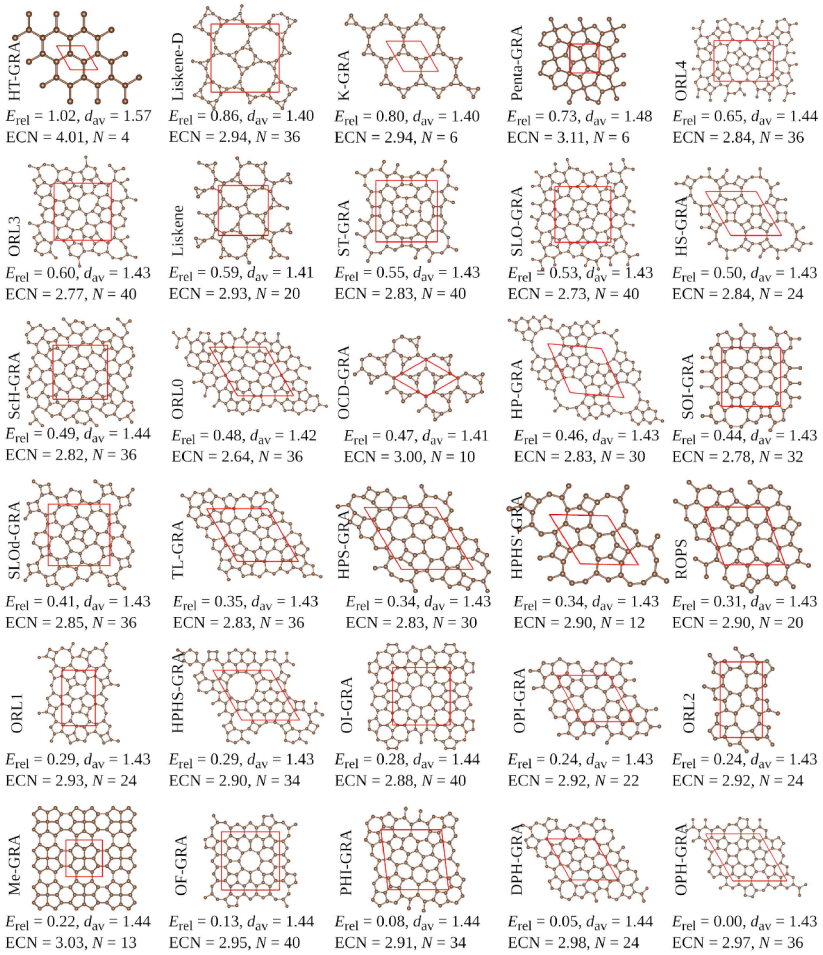

Figure 2. Unit cell of 2D carbon allotropes with complementary information about structural and energetic properties, where E_{rel} represents the relative total energy (eV/atom) from the lowest energy per atom allotrope, d_{av} (Å) denotes the average C−C bond length in each crystal structure, ECN signifies the effective coordination number, and N indicates the number of atoms in each unit cell.

frequencies were considered ST as local minima isomers. For instance, Figure 3 illustrates the phonon dispersions for the a-c configurations of OCD-GRA (a), Liskene (b), and Liskene-D (c), representing examples of ST, SS, and UN configurations, respectively. The complete set of phonon spectra can be found in the Supporting Information (Figures S1, S2, and S3). In the case of OCD-GRA, characterized as an ST configuration, the absence of negative frequencies confirms its mechanical stability. Conversely, for SS isomers such as Liskene, imaginary modes emerge in certain branches, such as at the M Brillouin zone point where vibrational modes are real. At the same time, they become imaginary along the X → Γ → Y path. Liskene-D exemplifies a UN configuration, wherein several modes are imaginary across all Brillouin zone branches.

Figure 4 illustrates the lattice parameters (a, b, and c) and their corresponding angles (α, β, and γ) for all of the studied carbon allotropes, along with the number of atoms in the unit cell ($N_{unit\ cell}$). Based on previous phonon dispersion analyses, the structures are classified as ST, SS, or UN according to the sequence of E_{rel} values. The carbon allotropes are classified into three unit cell shapes based on their a and b lattice vectors: diamond, squared, and rectangle. for configurations based on diamond and square units, $a = b$ is observed, while for rectangle-based configurations, $a \neq b$. Specifically, for square unit cells, $\alpha = \beta = \gamma = 90°$, whereas for diamond unit cells, $\alpha = \beta = 90°$, and γ exhibits slight deviations from 120°, with $\gamma <$ 120° (or >120°) observed for OPI-GRA and ROPS (HPS-GRA and HPHS'-GRA).

To assess the dynamic stability of the 14 ST and SS monolayers, we conducted DFTB-MD simulations. Thermalization experiments were initiated at 400 K (as a high temperature) for 10 ps, followed by a gradual decrease to 300 K over the same duration, mimicking the operational temperature of the solar cells. Figure 5 (a) confirms the thermodynamic stability of the ST and SS configurations, consistent with the phonon results. Moreover, the constancy of total energies under both temperature regimes indicates that the structures maintain their native topology within the canonical ensemble framework employed here, as observed in the first-principle calculations.

Taking into account the topological disparities among the ST and SS structures, we investigated the dynamic mobility of the C atoms using the root-mean-square deviation (RMSD), defined by the equation:

$$\mathrm{RMSD}_j = \sqrt{\frac{1}{n}\sum_{j=1}^{N}(x_j - x_k)^2} \quad (1)$$

for each x_j configuration corresponding to the j-frame throughout the j = 1, 2, 3, ..., 22000 frames obtained from molecular dynamics, where x_k is the reference configuration for every 50 frames, i.e., throughout k = 1, 50, 100, ... 21950. For

https://doi.org/10.1021/acsaem.4c01544
ACS Appl. Energy Mater. XXXX, XXX, XXX−XXX

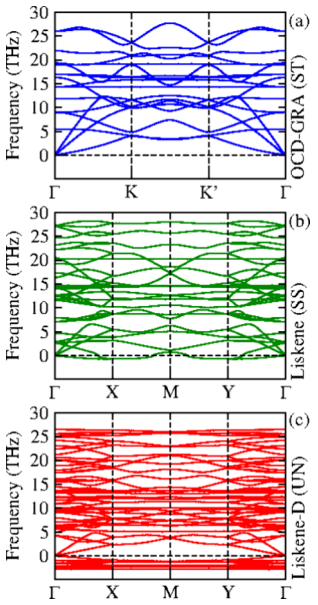

Figure 3. Examples of phonon dispersion for (a) stable (ST) - OCD-GRA, (b) semistable (SS) - Liskene, and (c) unstable (UN) - Liskene-D 2D carbon allotropes monolayers. Phonon dispersion for the other 2D carbon allotropes monolayers can be found in the Supporting Information.

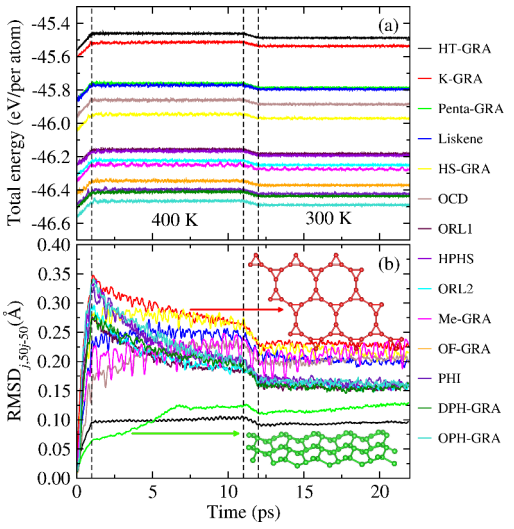

Figure 5. (a) Total energies (eV/per atom) for all the ST and SS configurations (HT-GRA, K-GRA, Penta-GRA, Liskene, HS-GRA, OCD, ORL1, HPHS, ORL2, Me-GRA, OF-GRA, PHI-GRA, DPH-GRA, and OPH-GRA) obtained through the Berendsen thermostat at 400 K and after thermalization at room temperature (300 K). (b) Root mean square deviation ($RMSD_j$) calculated for each j-frame throughout j = 1, 2, 3, ..., 22000. The K-GRA and Penta-GRA configurations are highlighted as the most and least susceptible to temperature effects, respectively.

instance, in the j = 1 → 50 interval, the reference frame is k = 1, while in the j = 51 → 100 interval, the reference frame is k = 50, and so on, as illustrated in Figure 5 (b). It becomes evident that ST and SS structures can be classified into three groups based on their behavior during the thermalization process at T = 300 K. For instance, K-GRA exemplifies configurations highly susceptible to temperature effects, exhibiting high mobility due to their open-like topology, primarily driven by the cyclic-carbonic chain (C_n) with n > 7. Examples include K-GRA (n = 12), Liskene (n = 10), HS-GRA (n = 12), and OCD-GRA (n = 8), all with RMSD > 0.20 Å. Conversely, HT-GRA and Penta-GRA represent the opposite extreme, demonstrating the lowest thermal susceptibility with RMSD < 0.15 Å, attributed to the presence of sp^3 sites conferring a certain level of rigidity to these structures. The most stable structures, such as OPH-GRA, DPH-GRA, and PHI, are intermediate between these extremes, which exhibit an RMSD of around 0.18 Å. Despite the absence of high-mobility cyclic-carbonic-chains with n = 7 and 8, the presence of aromatic

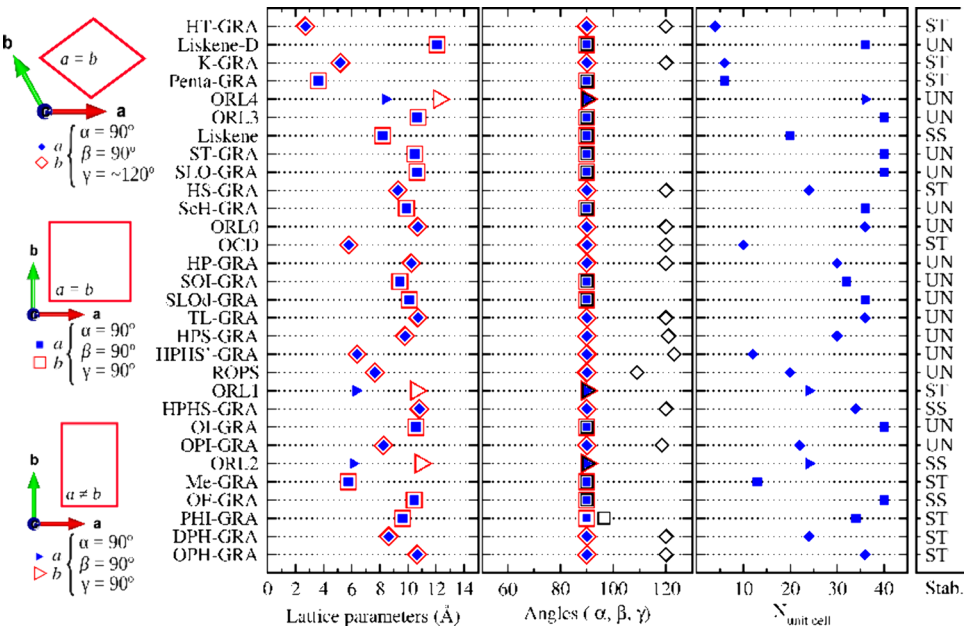

Figure 4. Unit cells are based on diamond (◇ with a = b, α = β = 90°, and γ ~ 120°), square (□ with a = b, α = β = γ = 90°), and rectangle (□, a ≠ b, α = β = γ = 90°) formats. The lattice parameters a and b (in Å) are listed on the left side; α, β, and γ angles are in the middle; and the number of atoms in the unit cell ($N_{\text{unit cell}}$) is on the right side. The classification of the isomers as ST, SS, and UN is highlighted for each allotrope.

https://doi.org/10.1021/acsaem.4c01544
ACS Appl. Energy Mater. XXXX, XXX, XXX−XXX

regions with n = 5 and 6 carbons imparts stability to the structure, mitigating the mobility induced by the cyclic-carbonic-chains.

3.2. Electronic Properties. In the electronic properties calculated for the 14 stable systems, it is observed that two allotropes exhibit metallic behavior (K-GRA and DPH-GRA), while the remaining are semiconductors, as depicted in the electronic band structures shown in Figure 6(a)−(n). The fundamental (E_g) and direct band gaps (E_g^d) at the HSE06 level are summarized in Table 1.

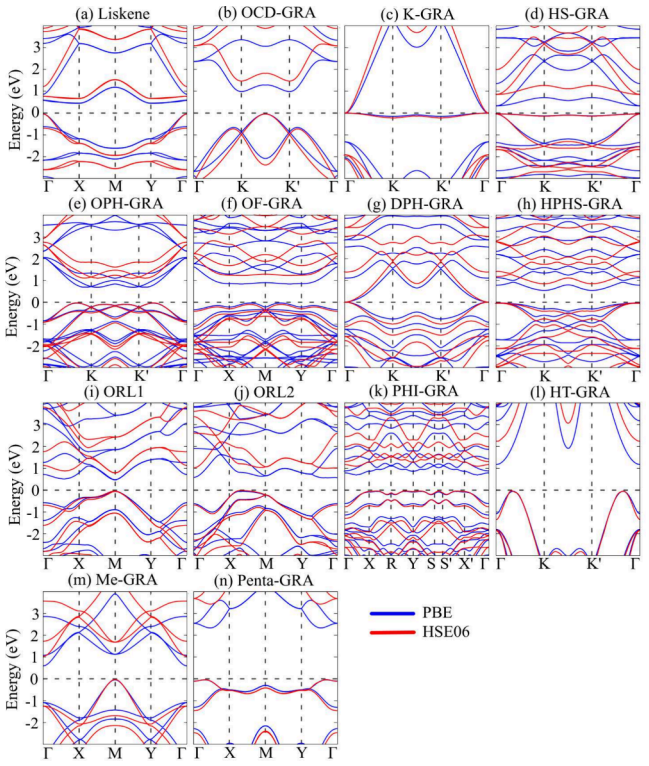

Figure 6. Electronic band structures for stable 2D carbon allotropes: (a) Liskene, (b) OCD-GRA, (c) K-GRA, (d) HS-GRA, (e) OPH-GRA, (f) OF-GRA, (g) DPH-GRA, (h) HPHS-GRA, (i) ORL1, (j) ORL2, (k) PHI-GRA, (l) HT-GRA, (m) Me-GRA, and (n) Penta-GRA, with PBE results in blue curves and HSE06 results in red curves.

Among the 12 semiconductor 2D carbon allotropes, only HS-GRA, OF-GRA, and ORL1 exhibit a fundamental direct band gap, while the rest are indirect band gap semiconductors. Despite that all systems are composed solely of carbon atoms, the electronic band gap varies within the range of 0.71 to 3.24 eV, highlighting a significant dependency of the electronic band gap on the structural properties and size of each C−C bond.

3.3. Excitonic and Optical Properties. Excitonic effects are fundamental in describing the linear optical response in 2D materials.[62] This study investigates these effects by solving the BSE for direct excitons (where the exciton momentum is zero; i.e., electron and hole pairs have the same momentum) and indirect excitons (with exciton momentum different from zero). Through the exciton band structure, as shown in the Supporting Information (section S9), we could identify the exciton ground state Ex_{gs} and the direct exciton ground state E_g^d, which also allows us to estimate the exciton binding energy, defined as $E_g - Ex_{gs}$. The data for all 12 semiconductor 2D carbon allotropes are presented in Table 1.

As expected, all indirect band gap 2D carbon allotropes have an indirect exciton ground state. Among the 3 direct band gap monolayers, two have a direct exciton ground state (OF-GRA and ORL1), while HS-GRA has an indirect excitonic ground state, which is not very common but can be justified by the orbital composition of the electron−hole pairs that compose the excitonic ground state wave function. This behavior, although uncommon, has been previously reported in the literature,[63,64] and the opposite scenario, where the system has an indirect band gap and a direct exciton ground state, has also been reported.[65] The exciton binding energy ranges from 83.44 to 574.74 meV, with the majority of our systems falling between 180 and 300 meV, as expected for 2D materials.[62,66,67] This demonstrates the significant role of these quasi-particle effects in describing the optical band gap. The presence of indirect excitonic ground states also indicates the possibility of phonon-assisted optical transitions, with absorption peaks at lower energies than the optical band gap. Through the oscillator strength, i.e., optical transition probability, we identified that all direct excitonic ground states are bright, meaning that they have an oscillator strength higher than 0.1 Å^2 for $\hat{x}$ or $\hat{y}$ linear light polarization.

Figure 7 (a)-(l) illustrates the linear optical response of the 12 semiconductor 2D carbon allotropes, considering linear light polarization in $\hat{x}$ (blue curves) and $\hat{y}$ (red curves) directions, at the IPA (dashed curves) and BSE (solid curves) levels of theory. A comparison of BSE and IPA absorption peaks highlights how excitonic quasi-particle effects significantly alter the linear optical response of these 2D materials. At the IPA level, which considers only single-particle states, ORL1, ORL2, and HT-GRA exhibit significant optical anisotropy, indicating different optical responses for $\hat{x}$ and $\hat{y}$ light polarizations. In ORL1 and ORL2, this difference is further pronounced for higher energy optical transitions. This optical anisotropy primarily stems from the atomic structure of these compounds combined with the orbital composition of valence and conduction states.

At the BSE level, the optical anisotropy observed in ORL1, ORL2, and HT-GRA persists, and it also emerges in the remaining semiconductor allotropes, underscoring the strength of excitonic quasi-particle effects. While optical anisotropy exists for most of these systems at the BSE level, it is not as pronounced except for those of OCD-GRA, ORL2, and HT-GRA. In these cases, the position of the first optical transition peak changes, suggesting the possibility of optical band gap engineering through incident light polarization.

3.4. Insights into Solar Harvesting Performance. The solar harvesting efficiency of our 12 2D carbon allotrope monolayers is estimated by calculating the PCE by using both the SQ-limit and SLME methods. The PCE is straightforwardly obtained from the monolayer's optical band gap in the SQ-limit approach. On the other hand, the SLME method considers additional factors such as layer thickness, the nature of the fundamental band gap (direct or indirect), and the monolayer absorption coefficient. Regardless of the method used for PCE calculation, it is crucial to note that the values obtained represent the upper limit of the solar harvesting efficiency. Achieving these values experimentally often requires years of investigation. For instance, the experimental PCE of $MAPbI_3$ perovskite has significantly increased over the past decade, from 3.8% to 25.2%.[68,69]

https://doi.org/10.1021/acsaem.4c01544
ACS Appl. Energy Mater. XXXX, XXX, XXX−XXX

Table 1. MLWF-TB+BSE Calculated Excitonic Properties and Power Conversion Efficiency (PCE): HSE06 Fundamental Band Gap, E_g, HSE06 Direct Band Gap, E_g^d, Exciton Ground State, Ex_{gs}, Direct Exciton Ground State, Ex_{gs}^d, and Exciton Binding Energy, Ex_b, Obtained from $E_g - Ex_{gs}$[a]

System	E_g	E_g^d	Ex_{gs}	Ex_{gs}^d	Ex_b	PCE		
	eV	eV	eV	eV	meV	SLME	$SLME_{max}$	SQ
HT-GRA	2.25	2.92	1.68	2.23	574.74	0.00	12.19	17.66
Penta-GRA	3.24	3.35	2.74	2.77	499.54	0.16	7.49	7.58
Liskene	0.71	0.81	0.63	0.72	83.44	0.43	17.52	22.86
HS-GRA	0.90	0.90	0.48	0.53	416.42	0.21	11.79	14.86
OCD-GRA	1.51	1.87	1.24	1.50	275.25	0.49	23.72	31.26
ORL1	0.84	0.84	0.65	0.65	187.79	0.43	19.90	19.90
HPHS-GRA	0.88	1.21	0.68	0.86	202.13	0.40	17.50	26.31
ORL2	1.02	1.15	0.75	0.86	273.38	0.40	20.67	26.28
Me-GRA	1.06	1.71	0.87	1.46	191.30	0.33	14.40	31.81
OF-GRA	1.24	1.24	0.93	0.93	308.64	0.67	29.30	29.30
PHI-GRA	1.11	1.21	0.78	0.88	328.95	0.48	22.34	27.25
OPH-GRA	1.14	1.18	0.84	0.85	296.81	0.79	25.54	25.71

[a]All direct exciton ground states are bright. The PCE values are estimated considering excitonic effects and the solar cell operating at 298.15 K, obtained at the Shockley−Queisser (SQ) limit, spectroscopy-limited maximum efficiency (SLME), and using SLME but considering that all incident photons are absorbed ($SLME_{max}$). These results at the IPA level are presented in Supporting Information Table S7.

The PCE estimates for SQ-Limit and SLME, considering excitonic effects, are presented in Table 1. The corresponding results at the IPA level are shown in Supporting Information, Table S7. Using the SQ-limit (PCE^{SQ}), the PCE at the IPA level ranges from 1.98% to 32.34%, while at the BSE level, it ranges from 7.58% to 31.26%. This indicates how excitonic effects in determining the optical band gap influence PCE^{SQ}. At the SQ-Limit, the maximum achieved PCE of 33% occurs in systems with a band gap close to 1.33 eV.[50] The changes observed in PCE^{SQ} are directly related to this, as systems where the BSE optical band gap approaches 1.33 eV tend to enhance PCE^{SQ}, while the opposite trend also occurs.

When considering the SLME approach, the PCE^{SLME} values decrease significantly, falling below 0.5%, regardless of whether the BSE or IPA levels of theory are used. These markedly lower values compared to those obtained using the SQ-limit (PCE^{SQ}) can be attributed to the small thickness of these monolayers. Consequently, they exhibit very low absorption rates, meaning that the material absorbs only a small fraction of the incident photons. This characteristic could render the material nearly transparent, which poses a significant challenge for the application of 2D materials in photovoltaic devices.

Indeed, the concept of light trapping techniques, as proposed by Jariwala et al.,[70] offers a promising solution to enhance the absorbance rate of 2D materials, potentially boosting their performance in solar harvesting applications. To address this, we reconsidered the estimation of PCE using the SLME method (PCE_{max}^{SLME}), approximating the absorbance curve by a Heaviside function. This assumption assumes that all photons with energy equal to or higher than the optical band gap are absorbed, providing a more realistic scenario for applying 2D materials in photovoltaic devices.

In our investigation, PCE_{max}^{SLME} ranges from 1.90% to 32.08% at the IPA level and 7.49% to 29.05% at the BSE level. For systems where the optical band gap equals the fundamental band gap (IPA) or exciton ground state (BSE), PCE_{max}^{SLME} is equal to PCE^{SQ}. Among our 12 monolayers, we identified 5 with PCE_{max}^{SLME} at the BSE level exceeding 20%: OCD-GRA, OPH-GRA, OF-GRA, ORL2, and PHI-GRA. These materials show promise for solar-harvesting applications.

4. CONCLUSION

Our comprehensive investigation examined various semiconductive 2D carbon allotropes' structural features, thermal stability, dynamical profiles, and excitonic properties. Utilizing phonon and molecular dynamics calculations, we identified several stable and semistable candidates, including configurations such as HT-GRA, K-GRA, Penta-GRA, Liskene, HS-GRA, OCD, ORL1, HPHS, ORL2, Me-GRA, OF-GRA, PHI-GRA, DPH-GRA, and OPH-GRA. We employed the Berendsen thermostat and correlated the topological profiles of the structures with RMSD analysis to characterize the high mobility of carbon atoms in configurations like K-GRA, Liskene, HS-GRA, and OCD-GRA. This mobility is attributed to the presence of large cyclic-carbon chains. Conversely, configurations such as HT-GRA and Penta-GRA exhibited lower mobility due to sp^3 sites, resulting in greater structural rigidity. Out of the initial 30 systems studied, 14 passed stability tests. Notably, K-GRA and DPH-GRA displayed metallic behavior. At the same time, the rest remained semiconductors with HSE06 band gaps typically ranging from 0.7 to 3.5 eV, with most having a band gap close to 1.0 eV. The observed excitonic effects were significant, with exciton binding energies ranging from 180 to 300 meV across most investigated monolayers. These quasi-particle effects also led to optical anisotropy in monolayers such as OCD-GRA, OF-GRA, and Penta-GRA. Regarding solar harvesting efficiency, certain monolayers, including OCD-GRA, ORL2, OF-GRA, PHI-GRA, and OPH-GRA, showed potential as photo absorbers, with an upper limit efficiency exceeding 20%. Our findings support the theoretical feasibility of utilizing 2D carbon allotropes as photo absorbers in solar harvesting devices. However, challenges remain, including developing synthesis routes for these materials and producing thin films on a large scale. Achieving these upper limits in solar harvesting efficiency may require years of further research. Our findings aim to catalyze deeper theoretical and experimental investigations into applying 2D carbon allotropes to photovoltaic devices. In addition, we know that machine learning algorithms, such as Bayesian optimization, can be used to explore a broader range of carbon allotropes. Leveraging these advanced algorithms within the framework of scientific

https://doi.org/10.1021/acsaem.4c01544
ACS Appl. Energy Mater. XXXX, XXX, XXX−XXX

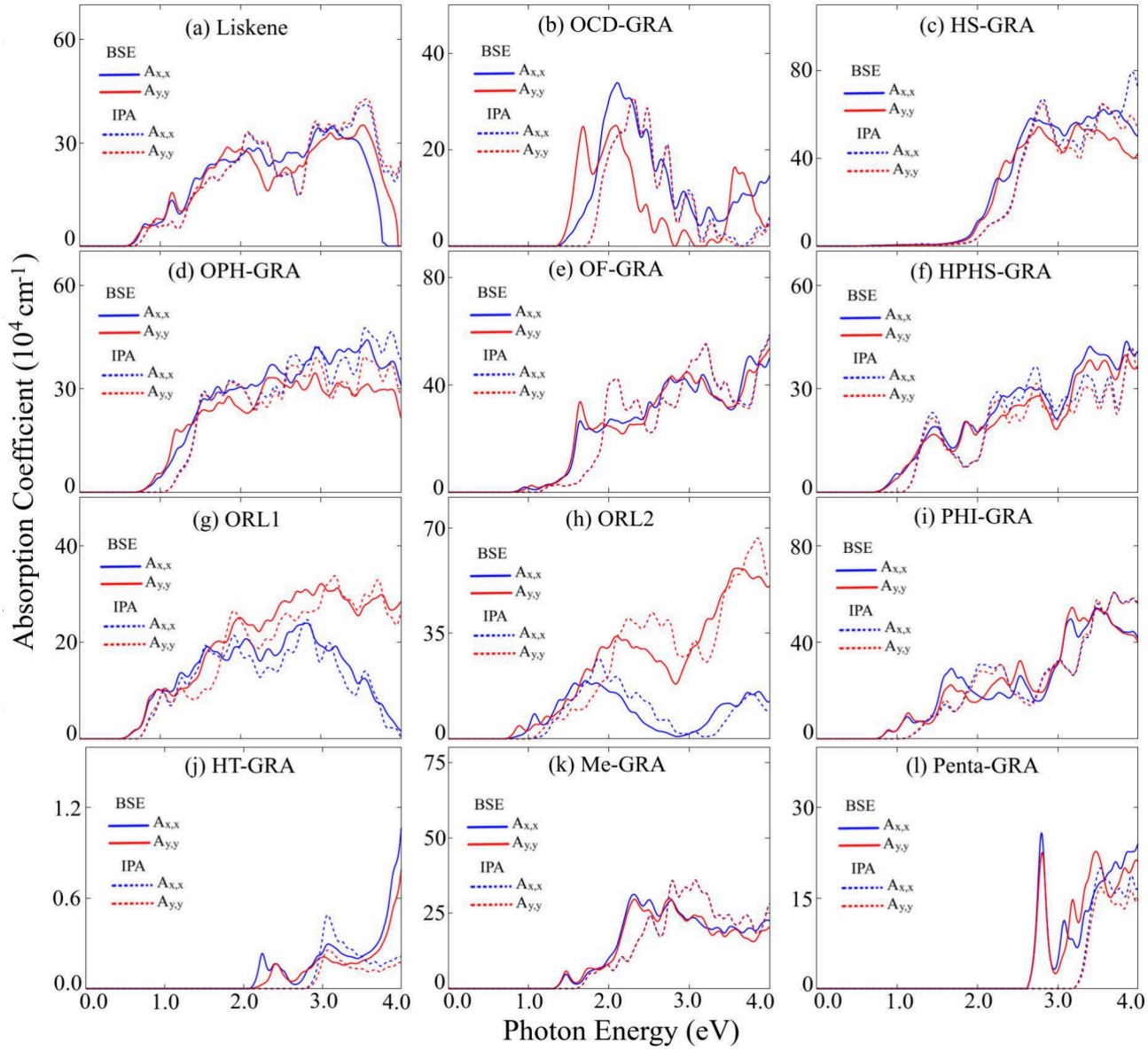

Figure 7. Absorption coefficient for stable 2D semiconductor carbon allotropes: (a) Liskene, (b) OCD-GRA, (c) HS-GRA, (d) OPH-GRA, (e) OF-GRA, (f) HPHS-GRA, (g) ORL1, (h) ORL2, (i) PHI-GRA, (j) HT-GRA, (k) Me-GRA, and (l) Penta-GRA, with BSE results as solid curves and IPA results as dashed curves. Blue curves represent linear light polarization along the $\hat{x}$ direction, while red curves represent linear light polarization along the $\hat{y}$ direction.

workflows can significantly enhance our ability to identify promising candidates efficiently. This approach will be a focal point of our upcoming project, aiming to expand the landscape of 2D carbon allotropes and accelerate the discovery of materials with superior properties for renewable energy applications.

■ ASSOCIATED CONTENT

Supporting Information

The Supporting Information is available free of charge at https://pubs.acs.org/doi/10.1021/acsaem.4c01544.

PAW projectors: computational technical details; 2D carbon allotropes name convention; structural data; POSCARs; high symmetry **k**-points; phonon dispersions; molecular dynamics stability; electronic band structure; excitonic and optical properties; and insights of solar harvesting efficiency (PDF)

■ AUTHOR INFORMATION

Corresponding Authors

Alexandre Cavalheiro Dias − *Institute of Physics and International Center of Physics, University of Brasília, Brasília 70919-970 Distrito Federal, Brazil;* orcid.org/0000-0001-5934-8528; Email: alexandre.dias@unb.br

Diego Guedes-Sobrinho − *Chemistry Department, Federal University of Paraná, CEP 81531-980 Curitiba, Brazil;* orcid.org/0000-0002-3313-2822; Email: guedessobrinho@ufpr.br

Authors

Carlos Derli Almeida Cornélio − *Institute of Physics, University of Brasília, Brasília 70919-970 Distrito Federal, Brazil; Departamento de Matemática, Universidade Estadual do Goiás, Fornosa 73807-250 Goiás, Brazil*

https://doi.org/10.1021/acsaem.4c01544
ACS Appl. Energy Mater. XXXX, XXX, XXX−XXX

Maurício Jeomar Piotrowski − *Department of Physics, Federal University of Pelotas, Pelotas, Rio Grande do Sul 96010-900, Brazil;* orcid.org/0000-0003-3477-4437

Luiz Antônio Ribeiro Júnior − *Institute of Physics, University of Brasília, Brasília 70919-970 Distrito Federal, Brazil; Computational Materials Laboratory, LCCMat, Institute of Physics, University of Brasília, 70910-900 Brasília, Brazil;* orcid.org/0000-0001-7468-2946

Carlos Maciel de Oliveira Bastos − *Institute of Physics and International Center of Physics, University of Brasília, Brasília 70919-970 Distrito Federal, Brazil*

Celso Ricardo Caldeira Rêgo − *Karlsruhe Institute of Technology (KIT), Institute of Nanotechnology, 76344 Eggenstein-Leopoldshafen, Germany;* orcid.org/0000-0003-1861-2438

Complete contact information is available at: https://pubs.acs.org/10.1021/acsaem.4c01544

Funding

The Article Processing Charge for the publication of this research was funded by the Coordination for the Improvement of Higher Education Personnel - CAPES (ROR identifier: 00x0ma614).

Notes

The authors declare no competing financial interest.

■ ACKNOWLEDGMENTS

The authors are thankful for financial support from the National Council for Scientific and Technological Development (CNPq, grant numbers 307345/2021-1, 408144/2022-0, and 305174/2023-1), Federal District Research Support Foundation (FAPDF, grant numbers 00193-00001817/2023-43 and 00193-00002073/2023-84), the Coordination for Improvement of Higher Level Education (CAPES), the Rio Grande do Sul Research Foundation (FAPERGS), and the German Federal Ministry of Education and Research (BMBF) for financial support of the project Innovation-Platform MaterialDigital (www.materialdigital.de) through project funding FKZ number: 13XP5094A. Part of this work was performed on the HoreKa supercomputer funded by the Ministry of Science, Research and the Arts Baden-Württemberg and by the Federal Ministry of Education and Research. In addition, the authors thank the "Centro Nacional de Processamento de Alto Desempenho em São Paulo" (CENAPAD-SP, UNICAMP/FINEP - MCTI project) for resources into the 897 and 570 projects, Lobo Carneiro HPC (NACAD) at the Federal University of Rio de Janeiro (UFRJ) for resources into 133 project C,IMATEC SENAI at Salvador − BA, Brazil for the partnership and support through the Atos Computer, and "Laboratório Central de Processamento de Alto Desempenho" (LCPAD) financed by FINEP through CT-INFRA/UFPR projects. L.A.R.J acknowledges the financial support from FAPDF grant 0193.000942/2015, CNPq grant 350176/2022−1, and FAPDF-PRONEM grant 00193.00001247/2021−20. A.C.D. and L.A.R.J also acknowledges PDPG-FAPDF-CAPES Centro-Oeste grant number 00193−00000867/2024−94. This paper was published under the CC BY Open Access license through the ACS-CAPES agreement. The authors gratefully acknowledge CAPES for the financial support provided for the publication of this work under the ACS-CAPES agreement.

■ REFERENCES

(1) Pang, J.; Mendes, R. G.; Bachmatiuk, A.; Zhao, L.; Ta, H. Q.; Gemming, T.; Liu, H.; Liu, Z.; Rummeli, M. H. Applications of 2D MXenes in energy conversion and storage systems. *Chem. Soc. Rev.* **2019**, *48*, 72−133.

(2) Khan, K.; Tareen, A. K.; Aslam, M.; Zhang, Y.; Wang, R.; Ouyang, Z.; Gou, Z.; Zhang, H. Recent advances in two-dimensional materials and their nanocomposites in sustainable energy conversion applications. *Nanoscale* **2019**, *11*, 21622−21678.

(3) Hutchison, J. E. Greener nanoscience: a proactive approach to advancing applications and reducing implications of nanotechnology. *ACS Nano* **2008**, *2*, 395−402.

(4) Novoselov, K. S.; Geim, A. K.; Morozov, S. V.; Jiang, D.-e.; Zhang, Y.; Dubonos, S. V.; Grigorieva, I. V.; Firsov, A. A. Electric field effect in atomically thin carbon films. *Science* **2004**, *306*, 666−669.

(5) Geim, A. K. Graphene: status and prospects. *Science* **2009**, *324*, 1530−1534.

(6) Xu, X.; Pereira, L. F. C.; Wang, Y.; Wu, J.; Zhang, K.; Zhao, X.; Bae, S.; Tinh Bui, C.; Xie, R.; Thong, J. T. L.; Hong, B. H.; Loh, K. P.; Donadio, D.; Li, B.; Özyilmaz, B. Length-dependent thermal conductivity in suspended single-layer graphene. *Nat. Commun.* **2014**, *5*, 3689.

(7) Sundqvist, B. Carbon under pressure. *Phys. Rep.* **2021**, *909*, 1−73.

(8) Tang, H.; Hessel, C. M.; Wang, J.; Yang, N.; Yu, R.; Zhao, H.; Wang, D. Two-dimensional carbon leading to new photoconversion processes. *Chem. Soc. Rev.* **2014**, *43*, 4281−4299.

(9) Xu, L.-C.; Wang, R.-Z.; Miao, M.-S.; Wei, X.-L.; Chen, Y.-P.; Yan, H.; Lau, W.-M.; Liu, L.-M.; Ma, Y.-M. Two dimensional Dirac carbon allotropes from graphene. *Nanoscale* **2014**, *6*, 1113−1118.

(10) Fan, X.; Li, J.; Chen, G. New carbon allotropes with metallic conducting properties: a first-principles prediction. *RSC Adv.* **2017**, *7*, 17417−17426.

(11) Withers, F.; Dubois, M.; Savchenko, A. K. Electron properties of fluorinated single-layer graphene transistors. *Phys. Rev. B* **2010**, *82*, 073403.

(12) Lu, H.; Li, S.-D. Two-dimensional carbon allotropes from graphene to graphyne. *J. Mater. Chem. C* **2013**, *1*, 3677−3680.

(13) Wang, Z.; Dong, F.; Shen, B.; Zhang, R.; Zheng, Y.; Chen, L.; Wang, S.; Wang, C.; Ho, K.; Fan, Y.-J.; Jin, B.-Y.; Su, W.-S. Electronic and optical properties of novel carbon allotropes. *Carbon* **2016**, *101*, 77−85.

(14) Enyashin, A. N.; Ivanovskii, A. L. Graphene allotropes. *Phys. Status Solidi B* **2011**, *248*, 1879−1883.

(15) Wang, Z.; Zhou, X.-F.; Zhang, X.; Zhu, Q.; Dong, H.; Zhao, M.; Oganov, A. R. Phagraphene: a low-energy graphene allotrope composed of 5−6−7 carbon rings with distorted dirac cones. *Nano Lett.* **2015**, *15*, 6182−6186.

(16) Tromer, R. M.; Machado, L. D.; Woellner, C. F.; Galvao, D. S. Thiophene-Tetrathia-Annulene monolayer (TTA-2D): A new 2D semiconductor material with indirect bandgap. *Physica E: Low-dim. Sys. and Nanostruc.* **2021**, *129*, 114586.

(17) Toh, C.-T.; Zhang, H.; Lin, J.; Mayorov, A. S.; Wang, Y.-P.; Orofeo, C. M.; Ferry, D. B.; Andersen, H.; Kakenov, N.; Guo, Z.; Abidi, I. H.; Sims, H.; Suenaga, K.; Pantelides, S. T.; Özyilmaz, B. Synthesis and properties of free-standing monolayer amorphous carbon. *Nature* **2020**, *577*, 199−203.

(18) Hou, L.; Cui, X.; Guan, B.; Wang, S.; Li, R.; Liu, Y.; Zhu, D.; Zheng, J. Synthesis of a monolayer fullerene network. *Nature* **2022**, *606*, 507−510.

(19) Fan, Q.; Yan, L.; Tripp, M. W.; Krejčí, O.; Dimosthenous, S.; Kachel, S. R.; Chen, M.; Foster, A. S.; Koert, U.; Liljeroth, P.; Gottfried, J. M. Biphenylene network: A nonbenzenoid carbon allotrope. *Science* **2021**, *372*, 852−856.

(20) Desyatkin, V. G.; Martin, W. B.; Aliev, A. E.; Chapman, N. E.; Fonseca, A. F.; Galvão, D. S.; Miller, E. R.; Stone, K. H.; Wang, Z.; Zakhidov, D.; Limpoco, F. T.; Almahdali, S. R.; Parker, S. M.; Baughman, R. H.; Rodionov, V. O. Scalable Synthesis and Characterization of Multilayer γ-Graphyne, New Carbon Crystals

with a Small Direct Band Gap. *J. Am. Chem. Soc.* **2022**, *144*, 17999−18008.
(21) Bafekry, A.; Faraji, M.; Fadlallah, M.; Jappor, H.; Karbasizadeh, S.; Ghergherehchi, M.; Gogova, D. Biphenylene monolayer as a two-dimensional nonbenzenoid carbon allotrope: a first-principles study. *J. of Phys.: Cond. Matter* **2022**, *34*, 015001.
(22) Rahaman, O.; Mortazavi, B.; Dianat, A.; Cuniberti, G.; Rabczuk, T. Metamorphosis in carbon network: From penta-graphene to biphenylene under uniaxial tension. *FlatChem.* **2017**, *1*, 65−73.
(23) Tromer, R. M.; Felix, L. C.; Ribeiro, L. A.; Galvao, D. S. Optoelectronic properties of amorphous carbon-based nanotube and nanoscroll. *Physica E: Low-dim. Sys. and Nanostruc.* **2021**, *130*, 114683.
(24) Felix, L. C.; Tromer, R. M.; Autreto, P. A.; Ribeiro Junior, L. A.; Galvao, D. S. On the mechanical properties and thermal stability of a recently synthesized monolayer amorphous carbon. *J. Phys. Chem. C* **2020**, *124*, 14855−14860.
(25) Pereira, M.; da Cunha, W.; de Sousa, R.; Nze, G. A.; Galvão, D.; Ribeiro, L. On the mechanical properties and fracture patterns of the nonbenzenoid carbon allotrope (biphenylene network): a reactive molecular dynamics study. *Nanoscale* **2022**, *14*, 3200−3211.
(26) Tromer, R. M.; Junior, L. A. R.; Galvão, D. S. A DFT study of the electronic, optical, and mechanical properties of a recently synthesized monolayer fullerene network. *Chem. Phys. Lett.* **2022**, *804*, 139925.
(27) Peng, B. Stability and strength of monolayer polymeric C60. *Nano Lett.* **2023**, *23*, 652−658.
(28) Rêgo, C. R. C.; Schaarschmidt, J.; Schlöder, T.; Penaloza-Amion, M.; Bag, S.; Neumann, T.; Strunk, T.; Wenzel, W. SimStack: An Intuitive Workflow Framework. *Frontiers in Mater.* **2022**, *9*, 9.
(29) Belavin, V.; Bulusheva, L.; Okotrub, A.; Tomanek, D. Stability, electronic structure and reactivity of the polymerized fullerite forms. *J. Phys. Chem. Solids* **2000**, *61*, 1901−1911.
(30) Hohenberg, P.; Kohn, W. Inhomogeneous Electron Gas. *Phys. Rev.* **1964**, *136*, B864−B871.
(31) Kohn, W.; Sham, L. J. Self-Consistent Equations Including Exchange and Correlation Effects. *Phys. Rev.* **1965**, *140*, A1133−A1138.
(32) Kresse, G.; Furthmüller, J. Efficient Iterative Schemes For *Ab Initio* Total-Energy Calculations Using a Plane-Wave Basis set. *Phys. Rev. B* **1996**, *54*, 11169−11186.
(33) Perdew, J. P.; Chevary, J. A.; Vosko, S. H.; Jackson, K. A.; Pederson, M. R.; Singh, D. J.; Fiolhais, C. Atoms, Molecules, Solids, and Surfaces: Applications of the Generalized Gradient Approximation for Exchange and Correlation. *Phys. Rev. B* **1992**, *46*, 6671−6687.
(34) Perdew, J. P.; Burke, K.; Ernzerhof, M. Generalized Gradient Approximation Made Simple. *Phys. Rev. Lett.* **1996**, *77*, 3865−3868.
(35) Cohen, A. J.; Mori-Sánchez, P.; Yang, W. Fractional charge perspective on the band gap in density-functional theory. *Phys. Rev. B* **2008**, *77*, 77.
(36) Crowley, J. M.; Tahir-Kheli, J.; Goddard, W. A. Resolution of the Band Gap Prediction Problem for Materials Design. *J. Phys. Chem. Lett.* **2016**, *7*, 1198−1203.
(37) Rêgo, C. R. C.; Tereshchuk, P.; Oliveira, L. N.; Da Silva, J. L. F. Graphene-supported Small Transition-metal Clusters: A Density Functional Theory Investigation Within van der Waals Corrections. *Phys. Rev. B* **2017**, *95*, 235422.
(38) Heyd, J.; Scuseria, G. E. Efficient hybrid density functional calculations in solids: Assessment of the Heyd-Scuseria-Ernzerhof screened Coulomb hybrid functional. *J. Chem. Phys.* **2004**, *121*, 1187−1192.
(39) Blöchl, P. E. Projector Augmented-Wave Method. *Phys. Rev. B* **1994**, *50*, 17953−17979.
(40) Elstner, M.; Porezag, D.; Jungnickel, G.; Elsner, J.; Haugk, M.; Frauenheim, T.; Suhai, S.; Seifert, G. Self-consistent-charge density-functional tight-binding method for simulations of complex materials properties. *Phys. Rev. B* **1998**, *58*, 7260−7268.
(41) Hourahine, B.; Aradi, B.; Blum, V.; Bonafé, F.; Buccheri, A.; Camacho, C.; Cevallos, C.; Deshaye, M. Y.; Dumitrică, T.; Dominguez, A.; Ehlert, S.; Elstner, M.; van der Heide, T.; Hermann, J.; Irle, S.; Kranz, J. J.; Köhler, C.; Kowalczyk, T.; Kubař, T.; Lee, I. S.; Lutsker, V.; Maurer, R. J.; Min, S. K.; Mitchell, I.; Negre, C.; Niehaus, T. A.; Niklasson, A. M. N.; Page, A. J.; Pecchia, A.; Penazzi, G.; Persson, M. P.; Řezáč, J.; Sánchez, C. G.; Sternberg, M.; Stöhr, M.; Stuckenberg, F.; Tkatchenko, A.; Yu, V. W.-z.; Frauenheim, T. DFTB+, a software package for efficient approximate density functional theory based atomistic simulations. *J. Chem. Phys.* **2020**, *152*, 152.
(42) Togo, A.; Tanaka, I. First principles phonon calculations in materials science. *Scripta Mater.* **2015**, *108*, 1−5.
(43) Gaus, M.; Goez, A.; Elstner, M. Parametrization and Benchmark of DFTB3 for Organic Molecules. *J. Chem. Theory Comput.* **2013**, *9*, 338−354.
(44) Berendsen, H. J. C.; Postma, J. P. M.; van Gunsteren, W. F.; DiNola, A.; Haak, J. R. Molecular dynamics with coupling to an external bath. *J. Chem. Phys.* **1984**, *81*, 3684−3690.
(45) Dias, A. C.; Silveira, J. F.; Qu, F. WanTiBEXOS: a Wannier based Tight Binding code for electronic band structure, excitonic and optoelectronic properties of solids. *Comput. Phys. Commun.* **2023**, *285*, 108636.
(46) Salpeter, E. E.; Bethe, H. A. A Relativistic Equation for Bound-State Problems. *Phys. Rev.* **1951**, *84*, 1232−1242.
(47) Mostofi, A. A.; Yates, J. R.; Lee, Y.-S.; Souza, I.; Vanderbilt, D.; Marzari, N. wannier90: A tool for obtaining maximally-localised Wannier functions. *Comput. Phys. Commun.* **2008**, *178*, 685−699.
(48) Rozzi, C. A.; Varsano, D.; Marini, A.; Gross, E. K. U.; Rubio, A. Exact Coulomb cutoff technique for supercell calculations. *Phys. Rev. B* **2006**, *73*, 73.
(49) *ASTM-G173-03 Standard Tables for Reference Solar Spectral Irradiances: Direct Normal and Hemispherical on 37° Tilted Surface*; ASTM International: West Conshohocken, PA, 2012. DOI: 10.1520/g0173-03r20.
(50) Shockley, W.; Queisser, H. J. Detailed Balance Limit of Efficiency of p-n Junction Solar Cells. *J. Appl. Phys.* **1961**, *32*, 510−519.
(51) Yu, L.; Zunger, A. Identification of Potential Photovoltaic Absorbers Based on First-Principles Spectroscopic Screening of Materials. *Phys. Rev. Lett.* **2012**, *108*, 068701.
(52) Silveira, J. F. R. V.; Besse, R.; Dias, A. C.; Caturello, N. A. M. S.; Silva, J. L. F. D. Tailoring Excitonic and Optoelectronic Properties of Transition Metal Dichalcogenide Bilayers. *J. Phys. Chem. C* **2022**, *126*, 9173−9184.
(53) Dias, A. C.; Bragança, H.; Lima, M. P.; Silva, J. L. F. D. First-principles investigation of the role of Cr in the electronic properties of the two-dimensional $Mo_xCr_{1-x}Se_2$ and $W_xCr_xSe_2$ alloys. *Phys. Rev. Materials* **2022**, *6*.
(54) Moujaes, E. A.; Dias, A. C. On the excitonic effects of the 1T and 1OT phases of PdS2, PdSe2, and PdSSe monolayers. *J. Phys. Chem. Solids* **2023**, *182*, 111573.
(55) Bernardi, M.; Palummo, M.; Grossman, J. C. Extraordinary Sunlight Absorption and One Nanometer Thick Photovoltaics Using Two-Dimensional Monolayer Materials. *Nano Lett.* **2013**, *13*, 3664.
(56) Shi, X.; Li, S.; Li, J.; Ouyang, T.; Zhang, C.; Tang, C.; He, C.; Zhong, J. High-Throughput Screening of Two-Dimensional Planar sp2 Carbon Space Associated with a Labeled Quotient Graph. *J. Phys. Chem. Lett.* **2021**, *12*, 11511−11519.
(57) Naseri, M.; Jalilian, J.; Salahub, D. R.; Lourenço, M. P.; Rezaei, G. Hexatetra-Carbon: A Novel Two-Dimensional Semiconductor Allotrope of Carbon. *Computation* **2022**, *10*, 19.
(58) Zhuo, Z.; Wu, X.; Yang, J. Me-graphene: a graphene allotrope with near zero Poisson's ratio, sizeable band gap, and high carrier mobility. *Nanoscale* **2020**, *12*, 19359−19366.
(59) Zhang, S.; Zhou, J.; Wang, Q.; Chen, X.; Kawazoe, Y.; Jena, P. Penta-graphene: A new carbon allotrope. *P. Natl. A. Sci.* **2015**, *112*, 2372−2377.

https://doi.org/10.1021/acsaem.4c01544
ACS Appl. Energy Mater. XXXX, XXX, XXX−XXX

(60) Inui, G. K.; Silveira, J. F. R. V.; Dias, A. C.; Besse, R.; Da Silva, J. L. F. Ab initio screening of two-dimensional CuQ_x and AgQ_x chalcogenides. *J. of Phys. Cond. Matter* **2022**, *34*, 305703.
(61) Hoppe, R. Effective Coordination Numbers (ECoN) and Mean Active Fictive Ionic Radii (MEFIR). *Z. Kristallogr.* **1979**, *150*, 23−52.
(62) Dias, A. C.; Bragança, H.; de Mendonça, J. P. A.; Silva, J. L. F. D. Excitonic Effects on Two-Dimensional Transition-Metal Dichalcogenide Monolayers: Impact on Solar Cell Efficiency. *ACS Appl. Energy Mater.* **2021**, *4*, 3265−3278.
(63) Santos, W. O.; Moucherek, F. M. O.; Dias, A. C.; Moreira, E.; Azevedo, D. L. Structural, optoelectronic, excitonic, vibrational, and thermodynamic properties of 1T'-OsO2 monolayer via ab initio calculations. *J. Appl. Phys.* **2023**, *134*, 074301.
(64) Santos, W. O.; Moucherek, F. M. O.; Dias, A. C.; Moreira, E.; Azevedo, D. L. 1T'-RuO2 monolayer: First-principles study of excitonic, optoelectronic, vibrational, and thermodynamic properties. *J. Mater. Res.* **2023**, *38*, 3677−3689.
(65) Lu, J.; Qu, F.; Zeng, H.; Cavalheiro Dias, A.; Bradão, D. S.; Ren, J. Intrinsic Valley Splitting and Direct-to-Indirect Band Gap Transition in Monolayer HfZrSiCO2. *J. Phys. Chem. Lett.* **2022**, *13*, 5204−5212.
(66) Haastrup, S.; Strange, M.; Pandey, M.; Deilmann, T.; Schmidt, P. S.; Hinsche, N. F.; Gjerding, M. N.; Torelli, D.; Larsen, P. M.; Riis-Jensen, A. C.; Gath, J.; Jacobsen, K. W.; Jørgen Mortensen, J.; Olsen, T.; Thygesen, K. S. The Computational 2D Materials Database: high-throughput modeling and discovery of atomically thin crystals. *2D Materials* **2018**, *5*, 042002.
(67) Gjerding, M. N.; Taghizadeh, A.; Rasmussen, A.; Ali, S.; Bertoldo, F.; Deilmann, T.; Knøsgaard, N. R.; Kruse, M.; Larsen, A. H.; Manti, S.; Pedersen, T. G.; Petralanda, U.; Skovhus, T.; Svendsen, M. K.; Mortensen, J. J.; Olsen, T.; Thygesen, K. S. Recent progress of the Computational 2D Materials Database (C2DB). *2D Materials* **2021**, *8*, 044002.
(68) Kojima, A.; Teshima, K.; Shirai, Y.; Miyasaka, T. Organometal Halide Perovskites as Visible-Light Sensitizers for Photovoltaic Cells. *J. Am. Chem. Soc.* **2009**, *131*, 6050−6051.
(69) Frolova, L. A.; Davlethanov, A. I.; Dremova, N. N.; Zhidkov, I.; Akbulatov, A. F.; Kurmaev, E. Z.; Aldoshin, S. M.; Stevenson, K. J.; Troshin, P. A. Efficient and Stable $MAPbI_3$-Based Perovskite Solar Cells Using Polyvinylcarbazole Passivation. *J. Phys. Chem. Lett.* **2020**, *11*, 6772−6778.
(70) Jariwala, D.; Davoyan, A. R.; Wong, J.; Atwater, H. A. Van der Waals Materials for Atomically-Thin Photovoltaics: Promise and Outlook. *ACS Photonics* **2017**, *4*, 2962−2970.

https://doi.org/10.1021/acsaem.4c01544
ACS Appl. Energy Mater. XXXX, XXX, XXX−XXX